



# Topology optimization of periodic structures for crash and static load cases using the evolutionary level set method

Hua-Ming Huang<sup>1</sup> · Elena Raponi<sup>1,2</sup> · Fabian Duddeck<sup>1</sup> · Stefan Menzel<sup>3</sup> · Mariusz Bujny<sup>3</sup>

Received: 31 January 2023 / Revised: 28 September 2023 / Accepted: 28 September 2023 /

Published online: 25 October 2023

© The Author(s) 2023

## Abstract

Assembly complexity and manufacturing costs of engineering structures can be significantly reduced by using periodic mechanical components, which are defined by combining multiple identical unit cells into a global topology. Additionally, the superior energy-absorbing properties of lattice-based periodic structures can potentially enhance the overall performance in crash-related applications. Recent research developments in periodic topology optimization (PTO) have shown its efficacy for tackling new design problems and finding advanced novel structures. However, most of these methods rely on gradient information in the optimization process, which poses difficulties for crash problems where analytical sensitivities are usually not directly applicable. In this paper, we present an effective periodic evolutionary level set method (P-EA-LSM) for the optimization of periodic structures. P-EA-LSM uses a low-dimensional level-set representation based on moving morphable components to parametrize a single unit cell, which is replicated in the design domain according to a predefined pattern. The unit cell is optimized using an evolutionary algorithm and the structural responses are calculated for the entire system. We initially assess the performance of P-EA-LSM using three 2D minimum compliance test cases with varying periodicities. Our results demonstrate that our approach produces solutions comparable to other state-of-the-art methods for PTO while keeping a low dimensionality of the optimization problem. Subsequently, we effectively evaluate the capabilities of P-EA-LSM in a crashworthiness scenario. This particular application highlights the significant potential of the method, which does not rely on analytical sensitivities.

---

✉ Hua-Ming Huang  
huaming.huang@tum.de

<sup>1</sup> Technische Universität München, Arcisstraße 21, 80333 Munich, Germany

<sup>2</sup> Sorbonne Université, CNRS, LIP6, Paris, France

<sup>3</sup> Honda Research Institute Europe GmbH, Carl-Legien-Straße 30, 63073 Offenbach am Main, Germany

**Keywords** Topology optimization · Periodic structure · Evolutionary algorithm · Level set method · Moving morphable components · Crashworthiness

## 1 Introduction

Topology optimization (TO) (Sigmund 2000; Bendsøe and Sigmund 2004; Sigmund and Maute 2013) aims at optimizing material distribution within a prescribed design space for a given set of objective functions and constraints. Several optimization criteria, such as structural compliance, natural frequencies, and heat conduction, are commonly used in industrial and engineering applications, where lightweight, low-cost, and high-performance structures are demanded.

The theory behind TO dates back to the classical work of Michell (1904). The first computer-based TO method was introduced by the pioneering work of homogenization method (Bendsøe and Kikuchi 1988; Hassani and Hinton 1998). Since then, several well-known TO approaches have been developed. The (SIMP) method (Bendsøe 1989; Bendsøe and Sigmund 1999; Sigmund 2001) assigns varying material densities to design elements and optimizes their distribution to achieve optimal structural performance while respecting material volume constraints. The evolutionary structural optimization (ESO) method (Xie and Steven 1993) is a computational design approach that draws inspiration from the principles of natural evolution to optimize structures for better performance and efficiency. The naive version of ESO involves gradually removing inefficient material with low stresses from the ground structure in a heuristic manner. However, the main problem of ESO is that prematurely removed elements are not able to be recovered due to the one-way element removal mechanism. As such, an improved version of ESO, often called bi-directional evolutionary structural optimization (BESO) (Querín et al. 1998; Yang et al. 1999; Querín et al. 2000; Huang and Xie 2007a), was later developed. The BESO method can remove elements from a structure iteratively while simultaneously adding efficient material back to the structure. The level set method (LSM) (van Dijk et al. 2013) has also emerged as a notable strategy. It employs a level-set function over a fixed computational domain to represent material and void regions. By manipulating this function, the method achieves topological changes seamlessly, providing a robust framework for exploring complex design spaces. The MMCs method (Guo et al. 2014; Zhang et al. 2015, 2017; Liu et al. 2018) is a versatile technique that allows concurrent optimization of material distribution and structural topology. It introduces deformable components or morphable elements with adjustable shapes, sizes, and orientations. During optimization, these components dynamically evolve, leading to intricate and innovative designs that surpass conventional methods. The smooth-edged material distribution for optimizing topology (SEMDOT) (Fu et al. 2020) uniquely combines an exploration of design space using perturbations and orthogonalization techniques with TO. Its ability to generate designs with smooth edges makes it particularly suitable for applications in architecture, industrial design, and other fields where both structural integrity and aesthetics are crucial. In addition, the non-penalization version of SEMDOT (Fu et al. 2023), characterized by the elimination of penalties on intermediate material densities, can yield improved results with stronger convergence,

compared to its penalized counterpart. This further emphasizes SEMDOT's utility in various engineering applications. Another impactful method is the floating projection topology optimization (FPTO) technique (Hu et al. 2020; Huang 2020, 2021). FPTO leverages advanced computational techniques to revolutionize material distribution within a given design space. The key innovation of FPTO lies in its floating projection strategy. Unlike traditional TO methods that rely on grid-based discretization, FPTO employs a continuous material distribution approach, allowing for smoother transitions between different materials. The majority of these techniques rely on finite element analysis (FEA) and progressively determine optimal topologies through iterative processes involving design variables denoting the presence of material within individual elements. However, this approach can incur significant costs that escalate exponentially with the complexity of the numerical models.

To reduce this complexity, structures with spatially repeated patterns are widely used in modern automotive and aircraft industries. Typical structures of such a type are often referred to as periodic structures, composed of a series of basic cells (units, modules). With the duplication of numerous identical unit cells, periodic structures provide significant advantages such as the ease of assembly, and, consequently, lead to lower manufacturing costs of mass production. By using periodic systems, one is able to optimize problems of larger scales that cannot be easily optimized as a whole, allowing for higher granularity and reducing computational costs. Furthermore, the favorable structural properties of energy absorption in periodic lattices (Deshpande et al. 2001; Tang et al. 2015; Mukhopadhyay and Adhikari 2016) can help to improve crashworthiness performance during impact events of moving vehicles.

Periodic cellular structures have garnered significant attention for crashworthiness applications due to their potential for achieving a combination of low volume and lightweight characteristics, coupled with attributes such as low peak acceleration, minimal displacement, and high energy absorption. Most of the used TO methods for periodic structures mentioned above utilize elemental sensitivity information to perform gradient-based search, and usually suffer from mesh-dependency issues (Sigmund and Petersson 1998). For some problems like crash TO, such approaches cannot be used directly since the analytical sensitivities are not available, and it is often also not possible to estimate them numerically due to the noisiness of the objective functions or constraints (Duddeck 2007).

Numerous studies suggest solutions that are based on empirical design, and the utilization of systematic design methods remains limited. To our knowledge, only a few exceptions are available in the literature. In the work by Najmon et al. (2018), the SIMP approach is employed to create compliant mechanism lattice (CML) based liners. Thus, the CML-based liners are designed for synthesizing rubber cellular unit cells within a comprehensive model that is subjected to ballistic simulation. Another study is proposed by Jia et al. (2021). They optimize the design of periodic cellular structure for crashworthiness based on the hybrid cellular automata (HCA) framework (Penninger et al. 2010; Mozumder et al. 2012), a biologically inspired algorithm, based on the evolution of a cellular automaton. However, it is fundamentally based on the heuristic assumption of energy homogenization, which limits its generalization.

In this paper, we present the periodic evolutionary level set method (PEA- LSM), a non-gradient macroscopic periodic topology optimization (PTO) method that does

not depend on the underlying finite element (FE) mesh. Thanks to the geometric representation scheme used by the proposed PTO approach, and the fact that only a single unit cell is subject to optimization, it is possible to keep the number of design variables at a very low level, which breaks the critical limitation of using evolutionary algorithms (EAs). The utilization of EAs enables optimization of any quantifiable objective functions, which makes the approach very general and applicable to a wide range of problems in structural TO (Bujny et al. 2018, 2021; Bujny 2020).

The remainder of this paper is organized as follows: Sect. 3 describes the solution strategies of the proposed PTO approach. Section 4 is devoted to the numerical setup and the analysis of results to assess the proposed method, using three 2D static examples from the literature. Section 5 evaluates the applicability of the proposed approach in the context of a 2D crash test case, demonstrating its effectiveness in handling gradient-free scenarios and showcasing its extended potential for addressing such complex problems. Section 6 summarizes the main findings of this paper and suggests topics for future research.

## 2 Related work

Traditional TO aims at finding an optimal material distribution within a design domain with minimal constraints, usually limited to a volume constraint. In contrast, PTO enforces a condition where the structure is composed entirely of repetitive unit cells, significantly limiting the design representation.

In general, there are two main streams in the research field of PTO related to the scale of the structures to be optimized: (1) Microstructures of material with infinite periodicals (Sigmund 1994a, b, 1995; Hassani and Hinton 1998) and (2) Macrostructures with finite periodicals (Huang and Xie 2007b; Zuo 2009; Chen et al. 2010; Xia et al. 2016; Thomas et al. 2020, 2021).

In the first case, periodic material design approaches are based on the assumption of periodic boundary conditions, since the micro-scale periodic structures are built on a base cell, which is an infinitesimal unit of the material, usually referred to as a periodic base cell (PBC). This makes it possible to analyze a single PBC of the material instead of the entire structure by FEA. In the context of micro-scale material optimization, PBCs have no specific physical size, and therefore, the optimized solution depends heavily on the scale effect of the unit cell (Xie et al. 2011). This becomes problematic when the optimized designs are to be manufactured.

In the second case, finite periodic optimization often utilizes the concept of an imaginary representative unit cell (RUC) (Huang and Xie 2007b; Zuo 2009), due to the fact that periodic structures comprising a finite number of identical components do not necessarily exhibit repeating boundary conditions across unit cells. In this scenario, the sizes of periodic components are often comparable to the characteristic length of the entire structural system. Consequently, the assumption of periodic boundary conditions over the material base cells is no longer valid since the stress and strain distributions are arbitrary (non-periodic) at the macro-structural level, even though the structural layout is periodic (Chen et al. 2017). Therefore, no scaling problems occur when transferring the optimization results to the production of the final product.

Although still in its infancy, finite periodic optimization at the macro-scale shows its applicability to a wide variety of structural systems such as architecture, bridges, aircraft, vehicles, etc. (Zuo 2009; Xia et al. 2016). Many works dealing with macrostructures with finite periodicals have emerged over the past years in the literature. To cite a few: Huang and Xie (2007b) proposed a method for the maximal stiffness (minimum compliance) of macroscopic periodic structures under a volume constraint using the BESO technique. The sensitivities are averaged at corresponding locations of each component and assigned to the RUC to satisfy the periodic constraint. Element removal/addition mechanism is executed based on the sensitivity ranking, and an iterative TO process is realized on the RUC. Ultimately, the optimized design of the whole periodic structure is constructed by duplicating the optimized RUC. Zuo (2009) enhanced the BESO approach by replacing void elements with soft material and developed the concept of sensitivity density for periodic structures that cannot be divided into equally-sized elements (e.g., cyclic periodic structures), to cope with the mesh-dependency problem caused by the non-uniform mesh. Chen et al. (2010) proposed a unified procedure for 3D multi-objective TO of finite periodic structures by considering a multi-physical problem of minimizing the mechanical and thermal compliance. Since constraints such as assembly conditions and the connection configuration of periodic sub-components are of particular importance in the real-world applications of PTO, Thomas et al. (2020) proposed to couple periodic optimization with common interfacing connections between periodic components, such as screws, welds, etc. This is frequently referred to as periodic multi-component optimization that deals with real assembly issues faced in real-world engineering designs. Thomas et al. (2021) presented a new methodology for the design of finite periodic structures by allowing variable orientation states for individual unit cells. Applying periodic optimization to these differently arranged repetitive cells may produce more efficient macro-structural designs than the conventional non-oriented (or translational) periodic counterparts, while maintaining the same degree of periodic constraints. This approach greatly expands the design space and takes more advantage of structural periodicity.

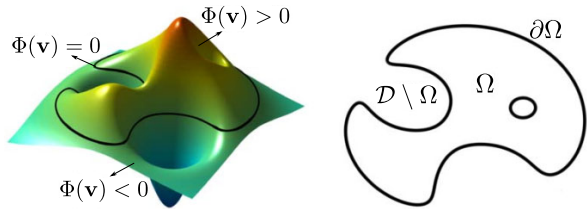
### 3 Periodic evolutionary level set method (P-EA-LSM)

In this section, we discuss the proposed methodology by addressing the geometry representation scheme (Sect. 3.1), periodic constraint handling (Sect. 3.2), problem formulation (Sect. 3.3), and optimization strategy (Sect. 3.4) of P-EA-LSM.

#### 3.1 Geometry representation

The parametrization of the design used by the P-EA-LSM is based on an implicit level-set description (van Dijk et al. 2013). The main idea of the LSM is to define the material distribution of a structure by means of a global level set function (LSF)  $\Phi$  as follows:

**Fig. 1** Illustration of the core concept in the LSM (Bujny et al. 2018)



$$\begin{cases} \Phi(\mathbf{v}) > 0, & \text{if } \mathbf{v} \in \Omega, \\ \Phi(\mathbf{v}) = 0, & \text{if } \mathbf{v} \in \partial\Omega, \\ \Phi(\mathbf{v}) < 0, & \text{if } \mathbf{v} \in \mathcal{D} \setminus \Omega, \end{cases} \quad (1)$$

where  $\mathbf{v} = [x, y]^T$  denotes the vector of Cartesian coordinates in a 2D design domain  $\mathcal{D} \in \mathbb{R}^2$ ,  $\Omega \subseteq \mathcal{D}$  is a subset of  $\mathcal{D}$ , representing the area occupied by the material phase,  $\mathcal{D} \setminus \Omega$  refers to the part of the design domain occupied by void, and, consequently,  $\partial\Omega$  is the interface between the material and void. It should be noted that the regions occupied by material and void correspond to positive and negative values of the LSF, respectively, and clear boundaries between material and void phases are precisely defined by the 0<sup>th</sup> iso-contour of the LSF, as shown in Fig. 1.

The global LSF is then composed of local LSFs, each representing an elementary beam component that can deform and move in the design domain. The local LSF  $\phi$  is defined as:

$$\begin{cases} \phi_i(\mathbf{v}) > 0, & \text{if } \mathbf{v} \in \Omega_i, \\ \phi_i(\mathbf{v}) = 0, & \text{if } \mathbf{v} \in \partial\Omega_i, \\ \phi_i(\mathbf{v}) < 0, & \text{if } \mathbf{v} \in \mathcal{D} \setminus \Omega_i, \end{cases} \quad (2)$$

where  $\Omega_i$  is the region occupied by the  $i$ th elementary component. As such, the total region of the design domain occupied by the material is given by:

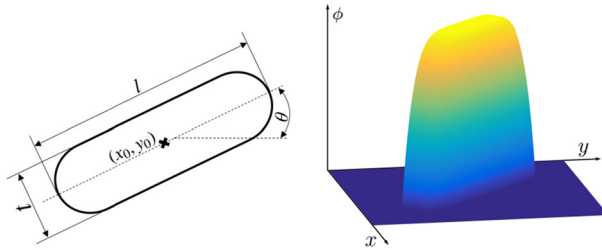
$$\Omega = \bigcup_{i=1}^{N_e} \Omega_i, \quad (3)$$

where  $N_e$  is the number of elementary components.

In particular, the LSF of each component can be described by special basis functions, which are often referred to as MMCs (Guo et al. 2014). In the MMC-based approach, several morphable structural components are adopted as basic building blocks of the topological design. Therefore, assuming that the design domain  $\mathcal{D}$  comprises  $N_e$  structural components made of solid material, it yields:

$$\Phi(\mathbf{v}) = \max(\phi_1(\mathbf{v}), \dots, \phi_i(\mathbf{v}), \dots, \phi_{N_e}(\mathbf{v})), \quad (4)$$

with  $\phi_i(\mathbf{v})$  denoting the local basis function of the  $i$ th component. For a design domain  $\mathcal{D} \in \mathbb{R}^2$  as in the present work, it takes the following form:



**Fig. 2** Parametrization of a single MMC (left) and the corresponding local LSF where negative values  $\phi < 0$  are set to zero (right) (Bujny et al. 2016)

$$\phi_i(\mathbf{v}) = - \left[ \left( \frac{\cos \theta_i \cdot (x - x_{0i}) + \sin \theta_i \cdot (y - y_{0i})}{l_i/2} \right)^q + \left( \frac{-\sin \theta_i \cdot (x - x_{0i}) + \cos \theta_i \cdot (y - y_{0i})}{t_i/2} \right)^q - 1 \right], \tag{5}$$

where  $q$  is a modeling exponent (equal to 6 in this paper),  $(x_{0i}, y_{0i})$ ,  $\theta_i$ ,  $l_i$ , and  $t_i$  denote the center coordinates, the inclined angle measured counterclockwise from the horizontal axis, and the length as well as thickness of the  $i$ th MMC, respectively. Figure 2 depicts the resulting parametrization of a single MMC and the corresponding local LSF according to Eq. (5). By modifying these five parameters, the optimizer can explicitly control the geometric features.

Once the geometric features of the structure are characterized by a set of LSFs, this description can be mapped to a fixed FE mesh with the use of a density-based geometry mapping, to compute the performance metrics via FEA. The geometry-mapping mechanism is employed to update the analysis model upon design changes. Hence, the relation between the global LSF  $\Phi$  and the element density  $\rho_e$  is defined as:

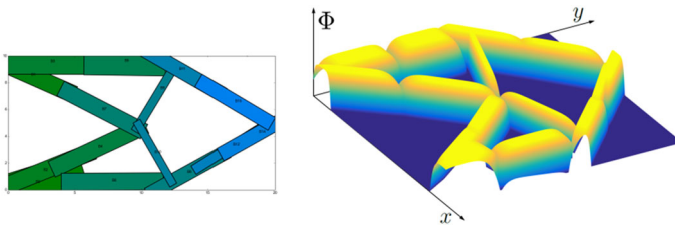
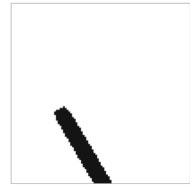
$$\rho_e = \rho(\mathbf{v}) = H(\Phi(\mathbf{v})), \tag{6}$$

where  $H(x)$  denotes the Heaviside function:

$$H(x) = \begin{cases} 0, & \text{if } x < 0 \\ 1, & \text{if } x \geq 0. \end{cases} \tag{7}$$

Therefore, P-EA-LSM restricts the element densities  $\rho(\mathbf{v})$  to two discrete values—either zero or one— which means that the design optimized by the P-EA-LSM is black-and-white (Fig. 3) and free from ambiguous, intermediate density as commonly encountered in the density-based TO methods (Bendsøe 1989; Bendsøe and Sigmund 1999; Sigmund 2001). This property is of very high importance for the manufacturability of the obtained topologies, and, is beneficial in case of some problems, e.g., crash simulations, where the plastic incompressibility of the intermediate-density material can lead to nonphysical behavior of the structures (Bujny 2020).

**Fig. 3** Black-and-white design containing a single MMC obtained with the P-EA-LSM



**Fig. 4** An example layout of the optimized structural components (*left*) and the corresponding global LSF where negative values  $\Phi < 0$  are set to zero (*right*) for the cantilever beam benchmark test case (Bujny et al. 2016)

The element density  $\rho_e = \rho(\mathbf{v})$  is in turn used to scale the stiffness tensor  $\mathbf{E}$ :

$$\mathbf{E}(\mathbf{v}) = \rho(\mathbf{v}) \cdot \mathbf{E}_0, \tag{8}$$

where  $\mathbf{E}_0$  is the reference stiffness tensor and  $\rho(\mathbf{v}) = 0$  or  $1$  is the element density at the point  $\mathbf{v} \in \mathcal{D}$ . It is worth noting that, in this paper, the so-called ersatz (weak) material model (Zhang et al. 2015) is used for FEA to prevent the stiffness matrix from becoming singular, and thus, improve numerical stability. More precisely, the empty regions are assigned a very small density value, which is not zero.

Within the above geometry representation scheme using MMCs, the layout of a structure can be parametrized exclusively by a vector of design variables:

$$\mathbf{x} = \left( (\mathbf{x}_1)^T, \dots, (\mathbf{x}_i)^T, \dots, (\mathbf{x}_{N_e})^T \right)^T, \tag{9}$$

where

$$\mathbf{x}_i = (x_{0i}, y_{0i}, \theta_i, l_i, t_i)^T. \tag{10}$$

The vector of design variables  $\mathbf{x}$  is a collection of parameters defining  $N_e$  basis functions. Figure 4 shows an example layout of the optimized structural components for the cantilever beam benchmark test case.

### 3.2 Periodicity constraint

For the design of periodic structures, the macroscopic distribution of the material must be periodic, even if the stress or strain distribution does not necessarily exhibit periodic characteristics. An effective way to realize periodicity is to limit the design domain to



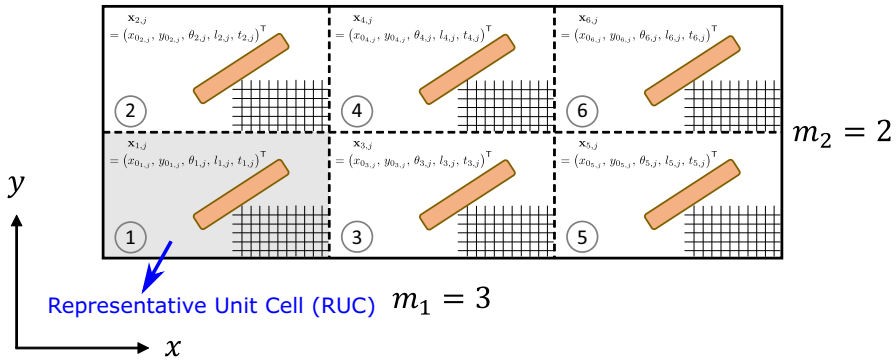


Fig. 5 An exemplary 2D design domain with a periodicity constraint and 6 (= 3 × 2) unit cells

a RUC. To achieve this, we can define the topology of periodic structures by the RUC that is to be replicated, such that the optimizer only has to modify the parameters of MMCs in the RUC.

In this paper, the design domain is divided into  $N_{UC} = m_1 \times m_2$  unit cells where  $m_1$  and  $m_2$  denote the numbers of unit cells along the x- and y-direction, respectively. For example,  $N_{UC} = 3 \times 2$  means that the design domain contains three unit cells in the x-direction and two unit cells in the y-direction, as shown in Fig. 5. The total number of unit cells  $N_{UC}$  is usually prescribed by the engineer’s design specifications. Please note that the special case of  $N_{UC} = 1 \times 1$  corresponds to the conventional TO problem.

### 3.3 Optimization problem

P-EA-LSM is built on the standard evolutionary level set method (EA-LSM), developed by Bujny (2020). The standard EA-LSM assumes the following form of optimization problems:

$$\begin{aligned}
 &\text{find} && \mathbf{x}, \\
 &\text{minimizing} && f_{\text{obj}}(\mathbf{x}), \\
 &\text{subject to} && \mathbf{r}(t) = \mathbf{0} \quad \text{and} \\
 &&& g_i(\mathbf{x}) \leq 0 \quad i = 1, \dots, n_{\text{ineq}},
 \end{aligned}
 \tag{11}$$

where  $\mathbf{x}$  is the vector of design variables,  $f_{\text{obj}}(\mathbf{x})$  is the objective function to be minimized, the residual  $\mathbf{r}(t) = \mathbf{0}$  expresses the mechanical equilibrium condition (static in case of compliance/stiffness optimization and dynamic at time  $t$  in case of crashworthiness optimization), and  $g_i(\mathbf{x})$  are the inequality constraints.

Since EAs are inherently unconstrained optimization methods, it is important to incorporate the constraints (frequently seen in the compliance/stiffness or crash applications) into the objective function. A common constraint-handling technique uses exterior penalty functions (Coello 2002; Rao 2019), i.e., it adds a penalized term to the objective function whenever any of the constraints is violated. The general formu-

lation of the exterior penalty function can be written as follows:

$$J(\mathbf{x}) = f_{\text{obj}}(\mathbf{x}) + \sum_{i=1}^{n_{\text{ineq}}} p_i \cdot \max(0, g_i(\mathbf{x})), \quad (12)$$

where  $J(\mathbf{x})$  is the expanded objective function with additional penalized terms (usually called the cost function),  $p_i$  are weighting factors which often take very large constant values, in order to immediately reject infeasible designs upon design changes by heavily penalizing them. It is worth mentioning that any number of constraints can be easily handled with the penalty method. Therefore, arbitrary quantifiable optimization criteria can be taken into account for the standard EA-LSM and its extensions, which is valuable for complex cases as encountered in crash or multiphysics TO.

In Sect. 4, the periodic design task is concerned with the minimization of the structural compliance  $C$  subject to a volume constraint. Therefore, the optimization problem of a periodic structure using the P-EA-LSM can be formulated as follows:

$$\begin{aligned} \text{find} \quad & \mathbf{x} = \left( (\mathbf{x}_{1,1})^T, (\mathbf{x}_{1,2})^T, \dots, (\mathbf{x}_{1,N_e})^T \right)^T, \\ \text{minimizing} \quad & C = C(\mathbf{x}), \\ \text{subject to} \quad & g_1(\mathbf{x}) \leq 0 \quad \text{and} \\ & \mathbf{x}_{1,j} = \mathbf{x}_{2,j} = \dots = \mathbf{x}_{N_{\text{UC}},j} \quad j = 1, \dots, N_e, \end{aligned} \quad (13)$$

where  $N_{\text{UC}}$  is the number of unit cells in the periodic structure,  $N_e$  is the number of MMCs in each unit cell,  $i$  and  $j$  are the unit cell index and the MMC index in a given unit cell, respectively, and  $\mathbf{x}_{i,j} = (x_{0i,j}, y_{0i,j}, \theta_{i,j}, l_{i,j}, t_{i,j})^T$  describes the design vector of the  $j$ th MMC in the  $i$ th unit cell ( $x_{0i,j}$  and  $y_{0i,j}$  are defined with respect to the local coordinate system within unit cells).

Furthermore, the additional periodic constraint is explicitly expressed as  $\mathbf{x}_{1,j} = \mathbf{x}_{2,j} = \dots = \mathbf{x}_{N_{\text{UC}},j}$  to enforce structural periodicity in the topology. Because of the periodicity requirement, the corresponding MMCs in different unit cells should be treated equally. In other words, if the geometry of an MMC in one unit cell is changed, the MMCs at the same position of all the other unit cells are altered simultaneously.

Moreover,  $g_1(\mathbf{x}) \leq 0$  is a volume inequality constraint, defined as:

$$g_1(\mathbf{x}) = N_{\text{UC}} \cdot V_i - V_f \cdot V_0 \leq 0 \quad (i = 1, \dots, N_{\text{UC}}), \quad (14)$$

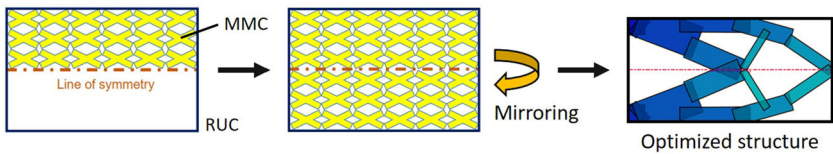
where  $V_i$  is the total volume of material in the  $i$ th unit cell,  $V_f$  is the required volume fraction, and  $V_0$  is the material volume of the entire design domain. The associated cost function  $J(\mathbf{x})$  in Eq. (12) reads:

$$J(\mathbf{x}) = C(\mathbf{x}) + P \cdot g_1(\mathbf{x}), \quad (15)$$

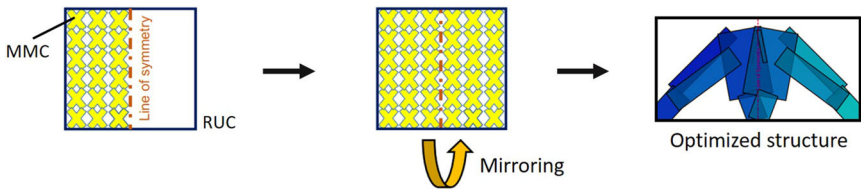
where  $P$  is the penalty factor for the volume inequality constraint.

It is worth pointing out that, in Eq. (13), the 1<sup>st</sup> unit cell is always selected as the RUC, and the design variables modify the topology of the RUC only. This reduces

### Horizontal symmetry



### Vertical symmetry

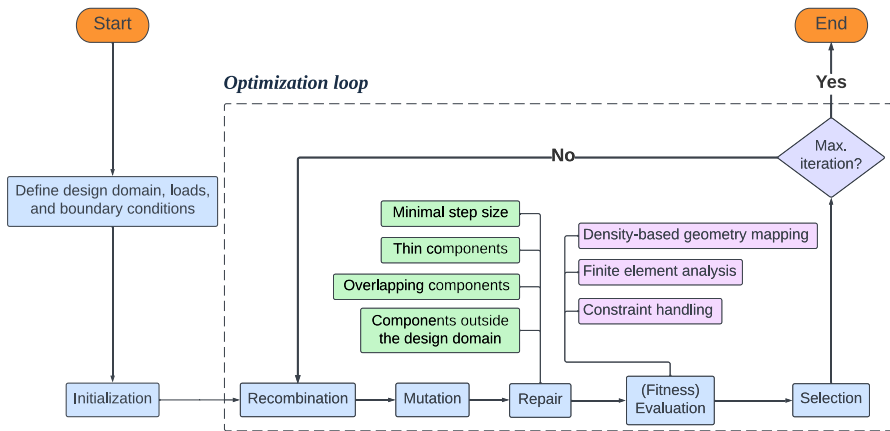


**Fig. 6** Conceptual diagram of horizontal and vertical symmetry conditions within the RUC

significantly the number of design variables in the optimization process. In addition, we can further reduce the number of design variables by imposing a horizontal or vertical symmetry condition within the RUC, thanks to the explicit geometrical information provided by the MMC-based framework in the P-EA-LSM. More specifically, as illustrated in Fig. 6, we can implement the symmetry conditions by defining the parameters of MMCs in one-half of the RUC, of which the other half is the reflection over the line of symmetry.

### 3.4 Optimization strategy

Figure 7 gives an overview of the P-EA-LSM in the form of a flowchart. The optimization procedure we present for PTO consists of the following steps. Firstly, as the preliminary phase, the design domain is defined with respect to the RUC, whereas the loads and boundary conditions are defined with respect to the macroscopic periodic topology. Then, P-EA-LSM starts with an initialization of the population of  $\mu$  parent individuals. Each of the parent individuals is characterized by a vector of design variables encoding the layout of level set basis functions. The strategy parameter used in ESs is also initialized in this step. Once the initial parent design is constructed, the algorithm enters the main optimization loop in which the iterative updating of structural topology is accomplished. In this work, we assume a fixed budget of FE evaluations. Thus, the optimization is performed until a maximum budget termination criterion is met. Next, the recombination operator combines the design vectors of  $\mu$  parent individuals to produce new  $\lambda$  offspring individuals. They are then modified by the mutation operator, which introduces random variations in the design vector to find better solutions in the neighborhood of given individuals. The mutation process depends on a single self-adapted step size (Schwefel 1987), meaning the algorithm controls the evolution of the strategy parameter itself during the optimization (or learning) process. To improve the quality of the obtained structures due to some unfavorable artifacts that occur during the optimization process, special repair operators are used



**Fig. 7** Flowchart of the numerical implementation using the P-EA-LSM. Note that the repair operators are used to deal with four different types of situations- for the sake of completeness, we refer the readers to the original work (Bujny 2020) for comprehensive descriptions

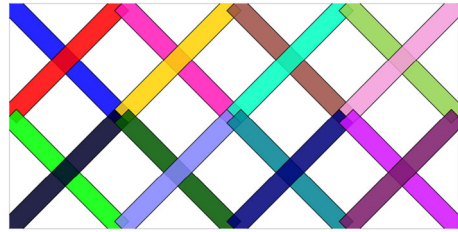
to handle different situations. Subsequently, the evaluation step involves the following stages: First, the density field of the RUC is mapped to a FE mesh via Eq. (6) and replicated to generate a large-scale FE mesh of the periodic structure depending on the periodicity specified by the engineer. Second, the evaluation function, i.e., FEA, rates the obtained solutions in terms of their fitness values, which reflect the quality of individual candidates. The fitness value is computed based on the violated constraints and the results from FE simulations (Eq. 12). One should note that the structural responses are evaluated for the entire periodic system containing multiple unit cells, since external boundary and loading conditions could substantially affect each component to different extents. Lastly, the selection operator picks a set of new candidates that compete based on their fitness for the next generation.

## 4 Validation of P-EA-LSM

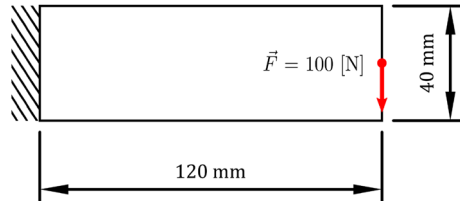
In this section, we present an extensive validation of the P-EA-LSM on 2D linear elastic problems over various periodicities. In the two first test cases considered in this section, representing typical benchmark scenarios used in the literature, we present a rigorous qualitative and quantitative comparison of the structures obtained using P-EA-LSM with periodic versions of the state-of-the-art density-based methods, SIMP and BESO. In addition, we demonstrate the capabilities of the proposed approach in a set of challenging scenarios aiming for optimization of 2D sandwich structures, which is an important practical application. Here, we include a qualitative comparison of the obtained structures with the ones from the literature, which are optimized using BESO technique.

Essentially, P-EA-LSM is a stochastic method due to the randomization used in the recombination and mutation operators. This implies that each optimization with the P-EA-LSM might bring slightly different solutions, and thus, a variety of final

**Fig. 8** Diagonal layout of MMCs used for the initial design, where the beams are evenly distributed throughout the 2D design domain



**Fig. 9** Design domain dimensions and boundary conditions for the clamped cantilever beam test case



compliance values for a given particular load case exists. Therefore, we performed multiple optimization runs for each test case to draw statistically sound conclusions about the performance of the optimized designs.

Previous experiments by Bujny (2020) have shown that diagonal layouts are preferred over other initial layouts of MMCs such as orthogonal or filled. Therefore, diagonal initial layouts are used in this paper (please see Fig. 8 for reference).

Throughout all the experiments in this section, the minimal step size used in the repair operator to avoid premature convergence of the optimization algorithm, and the step size used to distribute the initial population around the reference design, are taken as 0.005 and 0.03, respectively. In addition, the artificial Young's modulus assigned to the weak (ersatz) material for better numerical stability is set to  $1 \times 10^{-9}$ , and the penalty factor for the volume constraint is chosen as  $1 \times 10^{20}$ .

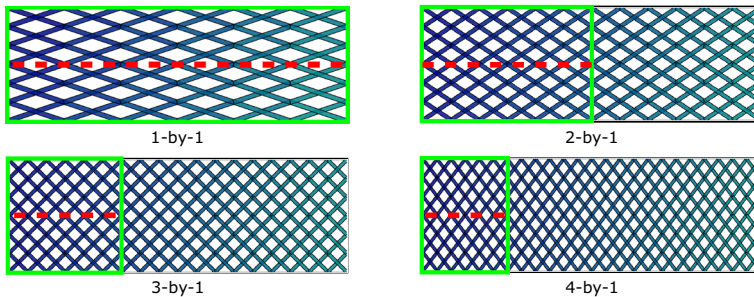
## 4.1 Clamped cantilever beam

### 4.1.1 Setup

Our first test case is the standard cantilever beam, with an external point load  $F$  applied at the middle point of the right edge. As shown in Fig. 9, the design domain dimensions are 120 mm by 40 mm. Within this design domain, the RUC is replicated to form periodic structures. The structural compliance  $C$  of the 1-by-1, 2-by-1, 3-by-1, and 4-by-1 periodic structures is minimized under a 60% volume constraint. The main numerical and optimization settings are provided in Table 1. One can note that within each of the unit cells, a horizontal symmetry condition is imposed, and a total number of 72 ( $= 6 \times 6 \times 2$ ) MMCs per unit cell after mirroring with 180 ( $= 6 \times 6 \times 5$ ) design variables is used for the initial design (Fig. 10).

**Table 1** Configuration and parameter settings for the clamped cantilever beam test case

Property	Symbol	Value	Unit
Young's modulus	$E$	$2.1 \times 10^5$	MPa
Poisson's ratio	$\nu$	0.3	–
External point load	$F$	100	N
Required volume fraction	$V_f$	60%	–
Parent population size	$\mu$	10	–
Offspring population size	$\lambda$	70	–
Mesh resolution	–	$120 \times 40$	–



**Fig. 10** Initial parent design of diagonal MMC layouts for the clamped cantilever beam test case, containing a total number of 72 basis functions within each unit cell (green box). (Color figure online)



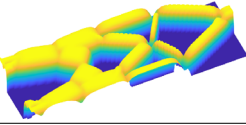


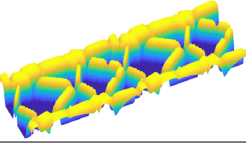


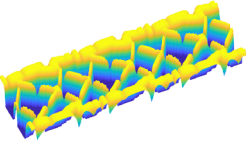


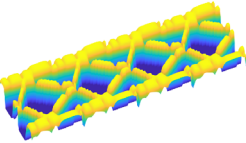
#### 4.1.2 Results

Table 2 presents the best designs chosen from 30 optimization runs for each periodic cantilever beam test case. MMC layouts and LSF plots are also provided along with the black-and-white material distribution for a better understanding of the underlying geometric features.

To validate our results, we used periodic versions of the state-of-the-art SIMP and BESO methods, whose MATLAB implementations were provided as supplementary material to the work of Thomas et al. (2021). The codes (Thomas 2021) were modified to account for rectangular shapes of the RUCs used in our paper. We used filtering radius of 1.5 mm and 2.0 mm in SIMP and BESO, respectively, and applied a threshold of 0.5 density to convert the resulting density fields to material or void and calculate the final compliance values. In the FE simulation model, in both cases we used the same parameters as indicated in Table 1.

Table 3 presents the best structures obtained using each of the methods and indicates relative change of compliance w.r.t. designs obtained with P-EA-LSM. One can observe that the designs from all the methods are qualitatively similar, showing the capability of the P-EA-LSM to optimize topologies of periodic structures. Surprisingly, in most cases, the method is able to find designs having lower compliance than the density-based approaches. However, the relative compliance difference in case of SIMP is negligible, and stays below 1%. Furthermore, additional investigations of topological attainability of the P-EA-LSM are realized in Table 4, by showing the cor-

**Table 2** Material distribution, layout of MMCs, and the global LSF corresponding to the best designs obtained in 30 optimization runs, for periodicities of 1-by-1, 2-by-1, 3-by-1, and 4-by-1, in the clamped cantilever beam test case

Periodicity ( $m_1, m_2$ )	Optimized periodic designs		
	Material distribution	MMC layout	LSF plot
(1, 1)			
(2, 1)			
(3, 1)			
(4, 1)			

The RUC is marked with a red box

responding best, median (15<sup>th</sup>), and worst designs among the 30 optimization runs for each of the periodic cantilever beam test cases.

Moreover, Fig. 11 shows the improvement in the compliance value over the first 500 iterations, corresponding to the best designs for the respective periodicity. It can be also noticed that, as shown in Fig. 12, the mean compliance value of periodic structures (2-by-1, 3-by-1, and 4-by-1) generally increases compared to the one of “non-periodic” structures, which implies that the conventional 1-by-1 structural design provides the best performance under the same loading and boundary conditions. This is an expected outcome, since imposing more constraints on a design usually results in decreased structural performance, but may contribute to better modularity or manufacturability.

**Table 3** Comparison of optimized periodic designs obtained with the P-EA-LSM and periodic versions of SIMP and BESO methods based on the codes published by Thomas et al. (2021), for the clamped cantilever beam test case

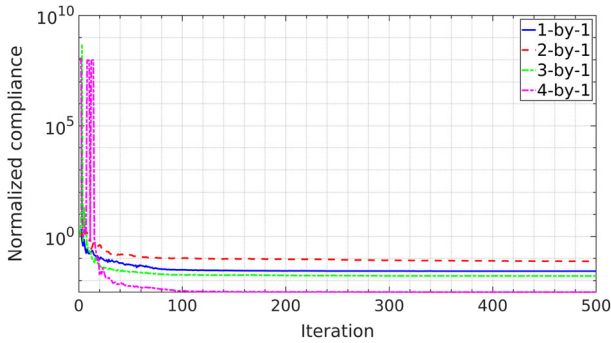
Periodicity ( $m_1, m_2$ )	Optimized periodic designs		
	P-EA-LSM	SIMP	BESO
(1, 1)	0.0%	-0.9%	-1.4%
(2, 1)	0.0%	+1.0%	+9.1%
(3, 1)	0.0%	+0.3%	+4.1%
(4, 1)	0.0%	+0.3%	+5.5%

For each periodicity, we show the optimized designs along with the relative compliance difference w.r.t. the best P-EA-LSM design  $\delta C = \frac{C - C_{P-EA-LSM}}{C_{P-EA-LSM}} \cdot 100\%$

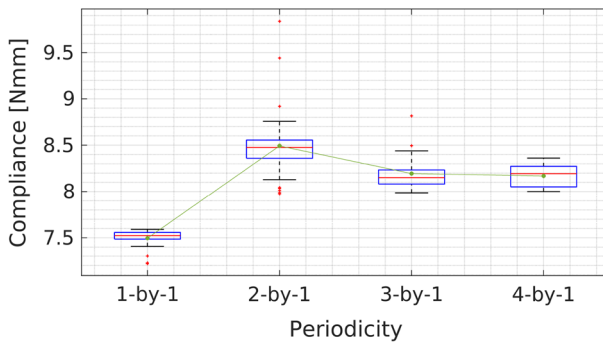
**Table 4** The best, median (15<sup>th</sup>), and worst designs out of 30 clamped cantilever beam optimizations obtained for periodicities of 1-by-1, 2-by-1, 3-by-1, and 4-by-1

Periodicity ( $m_1, m_2$ )	Periodic designs of clamped cantilever beams		
	Best	Median	Worst
(1, 1)			
(2, 1)			
(3, 1)			
(4, 1)			





**Fig. 11** Convergence plot illustrating the reduction of compliance values using a base-10 logarithmic scale over the first 500 iterations, corresponding to the best designs of periodic cantilever beams out of 30 optimization runs. The compliance values were normalized with the ones of the initial designs



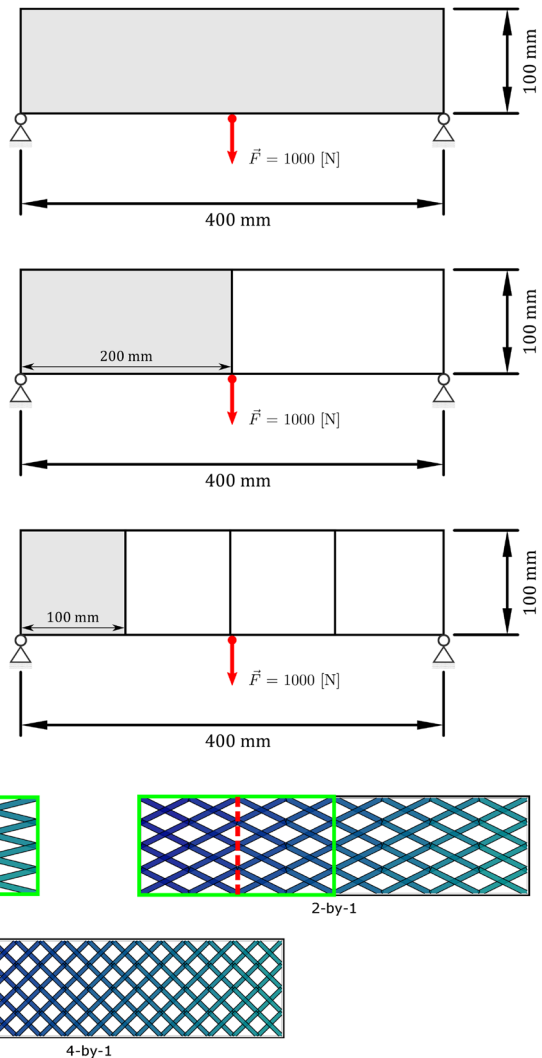
**Fig. 12** Distribution of 30 final compliance values in each box plot column for the clamped cantilever beam test case with periodicities of 1-by-1, 2-by-1, 3-by-1, and 4-by-1

## 4.2 Simply supported bridge

### 4.2.1 Setup

Another frequently considered test case is a 2D simply supported bridge structure, under a central point load  $F$  applied at the bottom edge. As depicted in Fig. 13, the bridge dimensions are  $400 \times 100$  mm, modeled with three different periodicities of 1-by-1, 2-by-1, and 4-by-1. Each unit cell in the respective periodic designs is composed of  $400 \times 100$ ,  $200 \times 100$ , and  $100 \times 100$  elements. A symmetry condition with respect to the vertical axis in each of the unit cells is also imposed, and a total number of 32 ( $= 4 \times 4 \times 2$ ) MMCs after mirroring with 80 ( $= 4 \times 4 \times 5$ ) design variables, is used for the initial configuration of each unit cell (Fig. 14). The periodic bridge structure is optimized by minimizing the structural compliance  $C$  subject to the prescribed volume constraint of 50%. A complete numerical setup is given in Table 5.

**Fig. 13** Design domain dimensions and boundary conditions for the periodic bridge structure, with periodicities of 1-by-1, 2-by-1, and 4-by-1



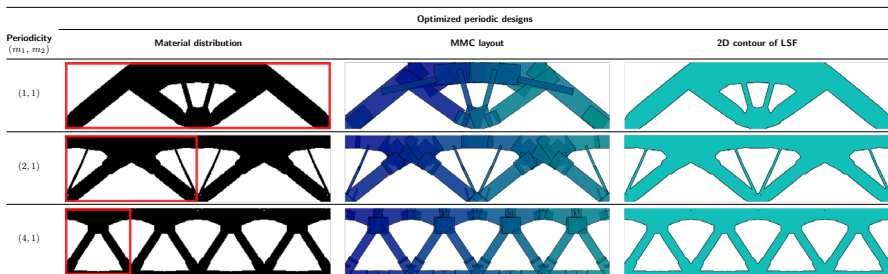
**Fig. 14** Initial parent design of diagonal MMC layouts for the simply supported bridge test case, containing a total number of 32 basis functions (i.e., MMCs) mirrored by the line of vertical symmetry (red dashed line) within each unit cell (green box). (Color figure online)

#### 4.2.2 Results

Table 6 illustrates the best optimized  $m_1$ -by- $m_2$  periodic bridge structures chosen from the 30 P-EA-LSM optimization runs. In Table 7, the results of the P-EA-LSM are compared with the periodic versions of SIMP and BESO based on the modified MATLAB codes from the work of Thomas et al. (2021), as described in Sect. 4.1. Again, in the table we indicate the relative changes of compliance w.r.t. the P-EA-LSM design. It can be observed that the designs obtained with SIMP and BESO are

**Table 5** Configuration and parameter settings for the simply supported bridge test case

Property	Symbol	Value	Unit
Young's modulus	$E$	$2.1 \times 10^5$	MPa
Poisson's ratio	$\nu$	0.3	–
External point load	$F$	1000	N
Required volume fraction	$V_f$	50%	–
Parent population size	$\mu$	5	–
Offspring population size	$\lambda$	35	–
Mesh resolution	–	$400 \times 100$	–

**Table 6** Material distribution, layout of MMCs, and 2D contour of global LSF corresponding to the best designs obtained in 30 optimization runs, for periodicities of 1-by-1, 2-by-1, and 4-by-1, in the simply supported bridge test case










The RUC is marked with a red box

more complex than those from the P-EA-LSM, since the former operate on thousands of design variables defining the densities of FEs, allowing for much higher structural attainability of density-based methods, whereas the latter only deals with a much lower number of design variables parameterizing the geometric characteristics of the MMCs. Nevertheless, all of the structures are qualitatively similar and their compliance values differ by less than 3%. Unexpectedly, in case of (1,1) and (2,1) periodicities, the P-EA-LSM structures yield better performance than the designs obtained with SIMP.

Moreover, as pointed out in the work by Bujny (2020), the complexity of the structures in P-EA-LSM can be controlled by the number of MMCs (and the associated minimal thicknesses), i.e., it is expected that structures of higher complexity can be constructed as the number of MMCs increases. Alternatively, to control the structural complexity, one could also try to specify larger values for the parent and offspring population sizes, resulting in higher probabilities that the P-EA-LSM can come up a wide diversity of optimized designs. Another approach is to enforce the minimum number of (effective) components that appear in the structure by using an explicit structural complexity controlling mechanism (Zhang et al. 2017).

Furthermore, Fig. 15 depicts how the compliance value has converged over the first 500 iterations, for optimization runs corresponding to the best designs in each of the periodic cases. One can also see from the box plot in Fig. 16 that, in the most trivial case of a 1-by-1 “periodic” structure, the design achieves an optimized mean compliance of 111.65. In contrast, the resultant 2-by-1 and 4-by-1 optimized periodic topologies

**Table 7** Comparison of optimized periodic designs obtained with the P-EA-LSM and periodic versions of SIMP and BESO methods based on the codes published by Thomas et al. (2021), for the simply supported bridge test case

Periodicity ( $m_1, m_2$ )	Optimized periodic designs		
	P-EA-LSM	SIMP	BESO
$\delta C$	0.0%	+0.2%	-1.1%
(1, 1)			
$\delta C$	0.0%	+1.8%	-0.7%
(2, 1)			
$\delta C$	0.0%	-2.6%	-2.0%
(4, 1)			

For each periodicity, we show the optimized designs along with the relative compliance difference w.r.t. the best P-EA-LSM design  $\delta C = \frac{C - C_{\text{P-EA-LSM}}}{C_{\text{P-EA-LSM}}} \cdot 100\%$

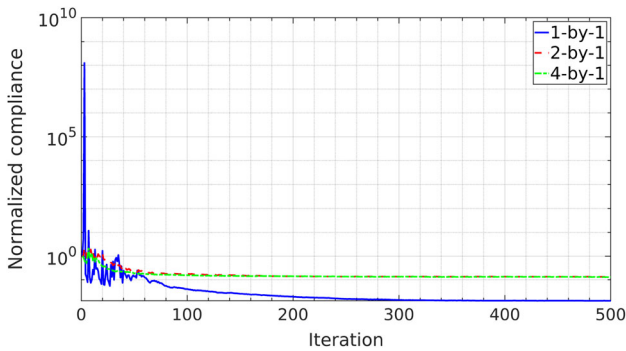
reach mean compliance of 131.02 and 169.81, meaning an increase of approximately 17% and 52%, respectively. This is due to the fact that enforcing structural periodicity, i.e., multiple identical substructures in a system, imposes additional constraints that must be satisfied by the optimization model, and, consequently, leads to growing final compliance values. More specifically, the periodic constraint requirement limits the design freedom and flexibility in the optimization procedure.

Based on the above observations, we can conclude that, in general, the value of the objective function (mean compliance) becomes higher as the total number of unit cells  $N_{\text{UC}}$  increases. Therefore, the solution of conventional TO corresponding to the limit case with  $N_{\text{UC}} = 1 \times 1$  has the lowest mean compliance value and best performance. However, the advantage of a periodic design is that it reduces significantly the manufacturing and construction costs. It is also worth highlighting that, periodic structures are generally more robust in the presence of loading uncertainties, since the periodic constraint allows the structural configurations to perform larger topological changes throughout the evolutionary process (Zheng et al. 2018).

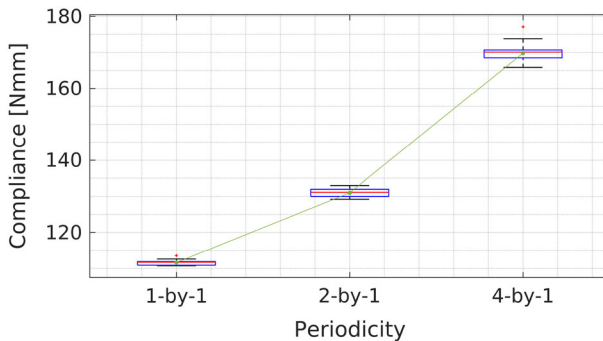
### 4.3 Sandwich structure

#### 4.3.1 Setup

The third test case is a design of the core of 2D sandwich structures, as described by Zhang and Sun (2006) and Huang and Xie (2007b). The rectangular design domain has dimensions  $L = 32$  mm and  $H_o = 20$  mm, with a height  $H_i = 16$  mm of designable core (Fig. 17).  $320 \times 200$  FEs are used to discretize the design domain. To avoid singularities in the FE model, a small non-designable passive element of width  $W = L/10000$  is added artificially along the right edge to transfer the applied load. The sandwich structure is fixed on the left edge, and uniform traction (force/length)  $F$  is applied on the right edge. We set a maximum volume fraction of 50% over the inner core area. For different test cases, the number of unit cells is increased steadily



**Fig. 15** Convergence plot illustrating the reduction of compliance values using a base-10 logarithmic scale over the first 500 iterations, corresponding to the best designs of periodic bridge structures out of 30 optimization runs. The compliance values were normalized with the ones of the initial designs



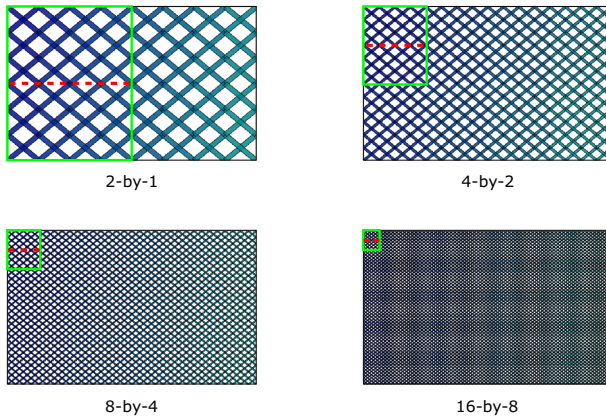
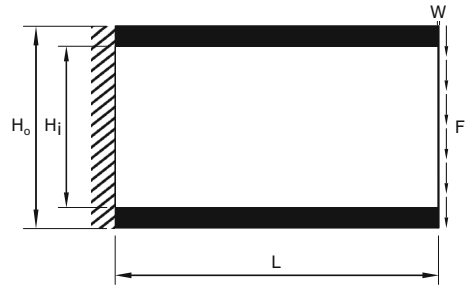
**Fig. 16** Distribution of 30 final compliance values in each box plot column for the simply supported bridge test case with periodicities of 1-by-1, 2-by-1, and 4-by-1

( $2 \times 1$ ,  $4 \times 2$ ,  $8 \times 4$ , and  $16 \times 8$ ) while keeping the structure size unchanged. Note that each unit cell in the respective periodic designs is composed of  $160 \times 200$ ,  $80 \times 100$ ,  $40 \times 50$ , and  $20 \times 25$  elements. Throughout the optimization process, symmetry of the periodic design is assumed with respect to the horizontal axis of symmetry of the domain, and a total number of 48 ( $= 4 \times 6 \times 2$ ) MMCs after mirroring with 120 ( $= 4 \times 6 \times 5$ ) design variables, is used per unit cell for the initial parent design (Fig. 18). Material properties ( $E$  and  $\nu$ ) and other input parameters are specified in Table 8.

### 4.3.2 Results

Table 9 presents the best results for the 30 runs for each of the respective periodicities, in conjunction with the literature results from the BESO method (Huang and Xie 2007b). Figures 19, 20, 21, and 22 present the evolution of topology, volume fraction, and objective function (compliance) for the periodic case of 2-by-1, 4-by-2, 8-by-4, and 16-by-8, respectively. It can be seen that the topology, volume fraction, and objective function are all converged at the end of the optimization process. In addition, we can

**Fig. 17** Design domain dimensions and boundary conditions for the optimization problem of the core design of a sandwich structure

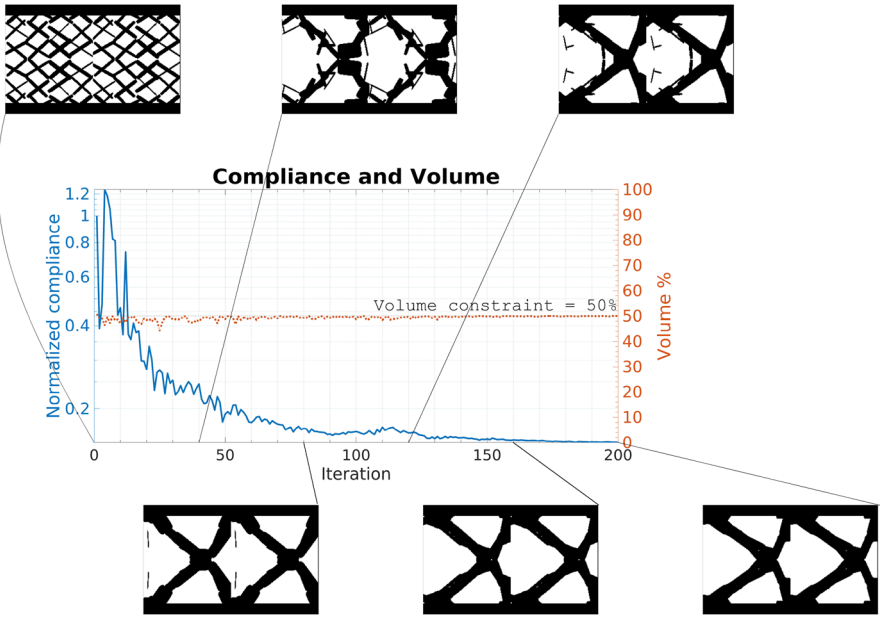


**Fig. 18** Initial parent design of diagonal MMC layouts for the core design of sandwich structures test case, containing a total number of 48 basis functions (i.e., MMCs) mirrored by the line of horizontal symmetry (red dashed line) within each unit cell (green box). (Color figure online)

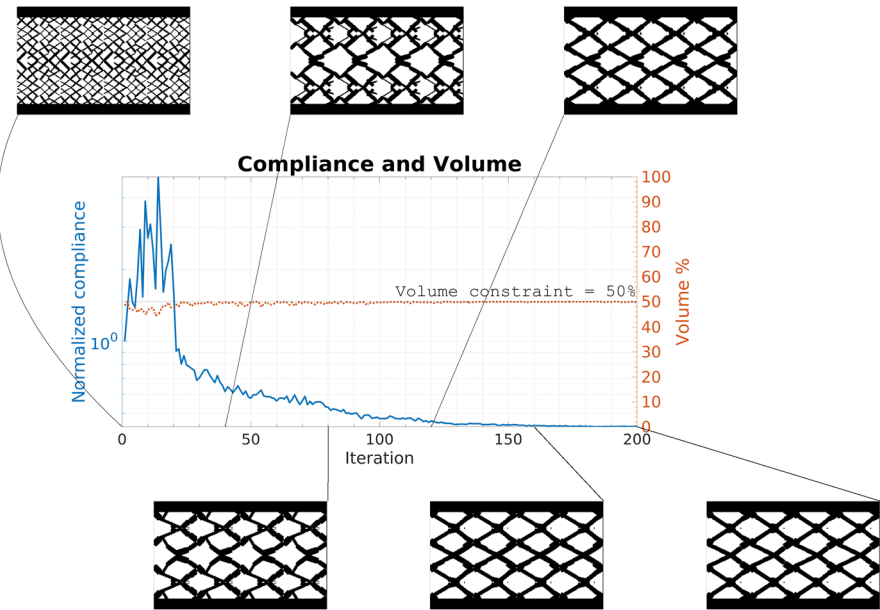
**Table 8** Configuration and parameter settings for the core design of sandwich structures test case

Property	Symbol	Value	Unit
Young's modulus	$E$	1000	MPa
Poisson's ratio	$\nu$	0.3	–
Uniform traction	$F$	100	$\frac{N}{mm}$
Required volume fraction	$V_f$	50%	–
Parent population size	$\mu$	5	–
Offspring population size	$\lambda$	35	–
Mesh resolution	–	$320 \times 200$	–

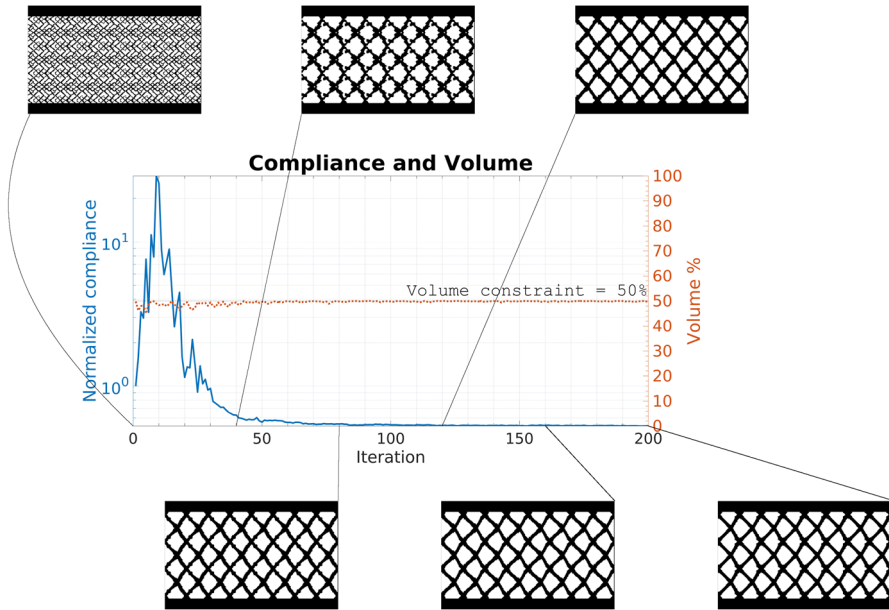
observe that, as the periodicity increases, the convergence of the topology is reached with fewer iterations. This can be attributed to a smaller design space for the RUC with increasing periodicity. Given the fixed number (48) of MMCs used per unit cell in the initial parent design, it is easier for the optimizer to compute the topologies, and thus, consume less computation time (in terms of iterations/generations).



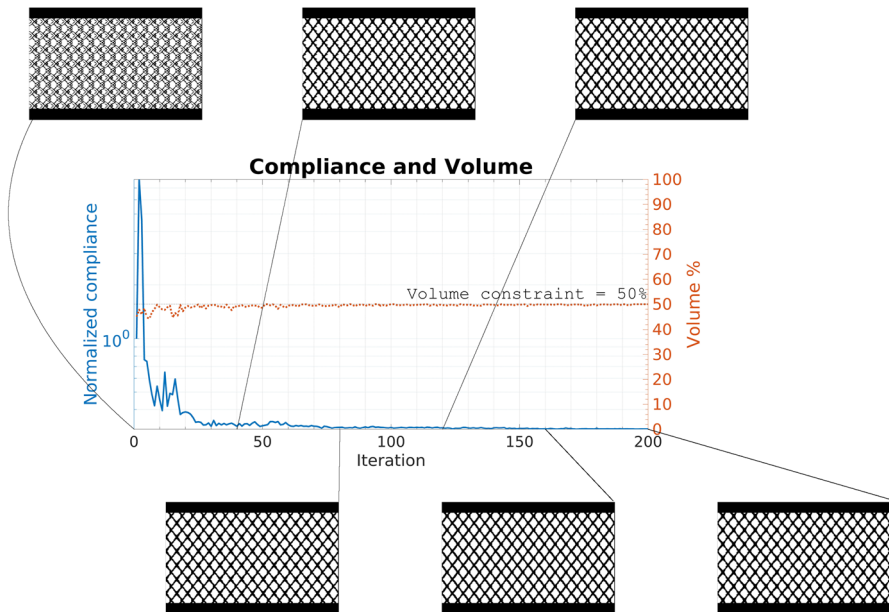
**Fig. 19** Evolution histories of topology, volume fraction, and compliance value (in a logarithmic scale) for the 2-by-1 periodic condition in the core design of sandwich structures test case. The compliance values were normalized with the ones of the initial designs



**Fig. 20** Evolution histories of topology, volume fraction, and compliance value (in a logarithmic scale) for the 4-by-2 periodic condition in the core design of sandwich structures test case. The compliance values were normalized with the ones of the initial designs



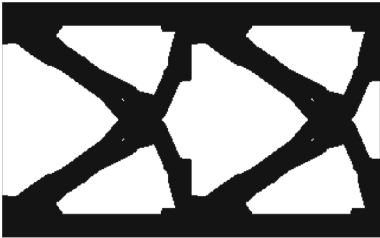
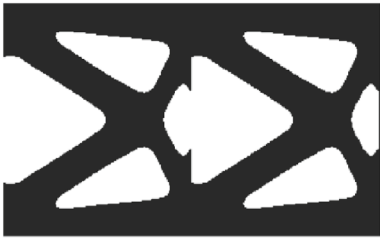
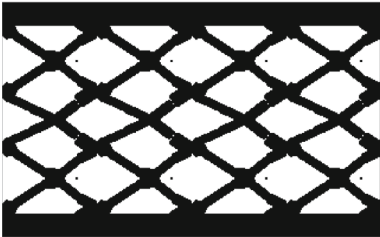

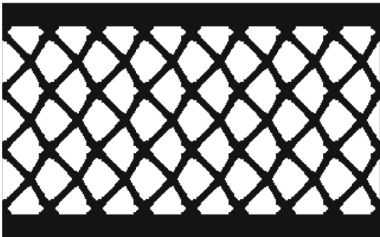
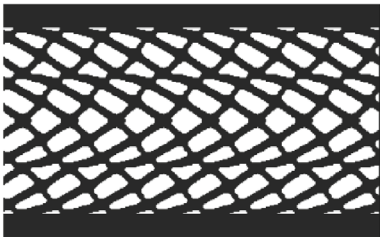
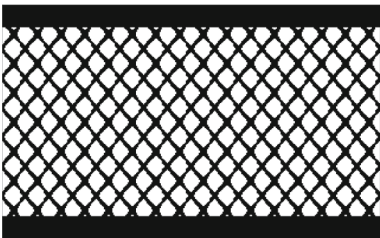
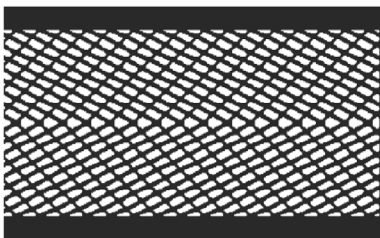
**Fig. 21** Evolution histories of topology, volume fraction, and compliance value (in a logarithmic scale) for the 8-by-4 periodic condition in the core design of sandwich structures test case. The compliance values were normalized with the ones of the initial designs



**Fig. 22** Evolution histories of topology, volume fraction, and compliance value (in a logarithmic scale) for the 16-by-8 periodic condition in the core design of sandwich structures test case. The compliance values were normalized with the ones of the initial designs



**Table 9** Comparison of optimized periodic designs obtained with the P-EA-LSM and BESO approach (Huang and Xie 2007b) for the core design of sandwich structures test case, with different periodic constraints

Periodicity ( $m_1, m_2$ )	Optimized periodic designs	
	P-EA-LSM	BESO
(2, 1)		
(4, 2)		
(8, 4)		
(16, 8)		

### 5 Evaluation on a crash numerical example

After validating the performance of P-EA-LSM on 2D linear elastic test cases with different periodicities, we proceed to evaluate the method on a 2D crash test case. In this scenario, sensitivity information is unavailable, rendering conventional gradient-based optimization algorithms inapplicable. Thus, the effectiveness of EAs, which

underpin our P-EA-LSM, in handling gradient-free scenarios becomes indispensable. Please note that the purpose of this section is not to conduct an extensive evaluation of the P-EA-LSM on crash-related problems. Instead, our primary aim is to demonstrate its extended applicability to these scenarios, where it can showcase its full potential.

The optimization problem we address is similar to the one presented in Sect. 4, but with a different objective function. Here, we analyze a transverse bending test case and minimize the intrusion  $d$  of an impactor into the structure. Therefore, the optimization problem is defined as follows:

$$\begin{aligned}
 &\text{find} && \mathbf{x} = \left( (\mathbf{x}_{1,1})^\top, (\mathbf{x}_{1,2})^\top, \dots, (\mathbf{x}_{1,N_e})^\top \right)^\top, \\
 &\text{minimizing} && d = d(\mathbf{x}), \\
 &\text{subject to} && \mathbf{r}(t) = \mathbf{0}, \\
 &&& g_1(\mathbf{x}) = N_{\text{UC}} \cdot V_i - V_f \cdot V_0 \leq 0 && i = 1, \dots, N_{\text{UC}}, \\
 &&& \mathbf{x}_{1,j} = \mathbf{x}_{2,j} = \dots = \mathbf{x}_{N_{\text{UC}},j} && j = 1, \dots, N_e,
 \end{aligned} \tag{16}$$

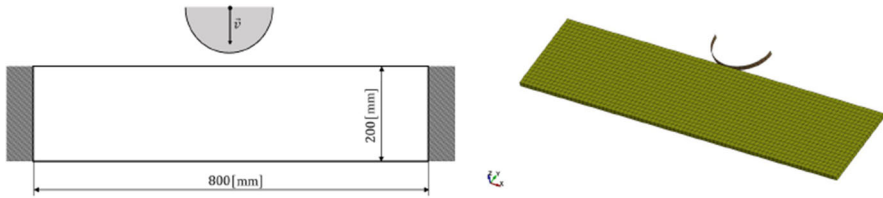
where the active constraint is still chosen as the total volume of the structure to be lower than or equal to the 50% of the design domain volume. The term  $\mathbf{r}(t) = \mathbf{0}$  expresses dynamic equilibrium at time  $t$ .

## 5.1 Setup

Our dynamic test is a transverse bending case, as shown in Fig. 23 (left). In this scenario, a pole impacts a beam that is supported at both ends and it generates an external dynamic load applied at the midpoint of its upper edge. The dimensions of the design domain are 800 mm by 200 mm. Within this area, the RUC is replicated to create periodic layouts. The goal is to minimize the intrusion of the impacting pole into the periodic structure. Three configurations are considered: 1-by-1, 2-by-1, and 4-by-1 periodic layouts. These configurations aim to achieve intrusion minimization while adhering to a volume constraint of 50%.

For the crash simulation, we rely on the commercial FEA software LS-DYNA (Isd 2014). As illustrated on the right of Fig. 23, the LSF is mapped on a reference LS-DYNA mesh composed of 6400 8-node solid elements with a piecewise linear plasticity material. The elements are subjected to a translational constraint in z-direction and rotational constraint about x- and y-axis. The numerical setup is provided in Table 10.

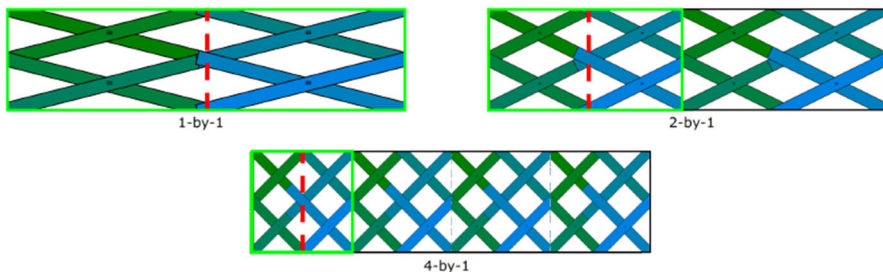
It is important to note that, within each unit cell, a vertical symmetry condition is enforced to reduce the dimensionality of the problem. Furthermore, for the initial design, a total of 8 MMCs are positioned in each unit cell according to a cross-shaped layout (see Fig. 24). As described by Eq. (5), each MMC is defined by 5 parameters, leading to 20 optimization variables in total.



**Fig. 23** Transverse bending test case: design domain dimensions and boundary conditions (*left*) and LS-DYNA FEM mesh (*right*)

**Table 10** Configuration and parameter settings for the transverse bending test case

Property	Symbol	Value	Unit
Young’s modulus	$E$	$7.0 \times 10^4$	MPa
Poisson’s ratio	$\nu$	0.33	–
Pole velocity	$v$	20	m/s
Pole mass	$m$	5.9	kg
Pole diameter	$D$	139.154	mm
Required volume fraction	$V_f$	50%	–
Mesh resolution	–	$160 \times 40$	–
Termination time	$t_{end}$	1.5	ms
Solver	–	LS-DYNA R7.1.1	–
Element type	–	8-node solid element	–

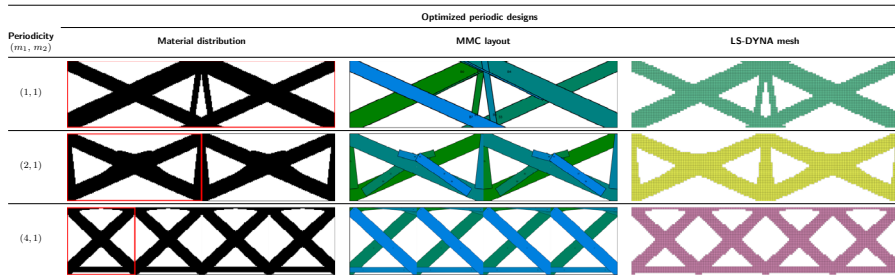


**Fig. 24** Initial parent design of diagonal MMC layouts for the pole intrusion test case, containing a total number of 8 ( $= 2 \times 2 \times 2$ ) basis functions (i.e., MMCs) mirrored by the line of vertical symmetry (*red dashed line*) within each unit cell (*green box*). (Color figure online)

### 5.2 Results

Table 11 presents the best designs from 10 optimization runs for each periodic transverse bending test case. The material distributions over the design space, along with the MMCs layouts and the LS-DYNA meshes are displayed. It is evident that the optimization runs enforcing either a 1-by-1 (i.e., no periodicity) or a 2-by-1 periodicity converge towards highly similar layouts. These layouts are in line with optima typically reported in the literature for non-periodic transverse bending test cases (Bujny

**Table 11** Material distribution, layout of MMCs, and LS-DYNA mesh corresponding to the best designs obtained in 10 optimization runs, for periodicities of 1-by-1, 2-by-1, and 4-by-1, in the transverse bending test case

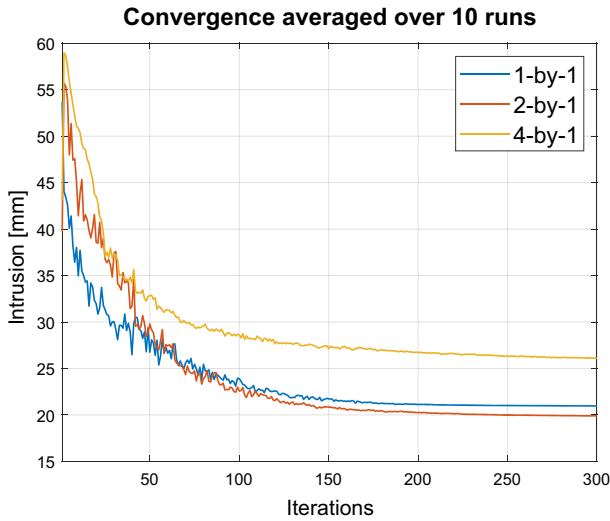


The RUC is marked with a red box

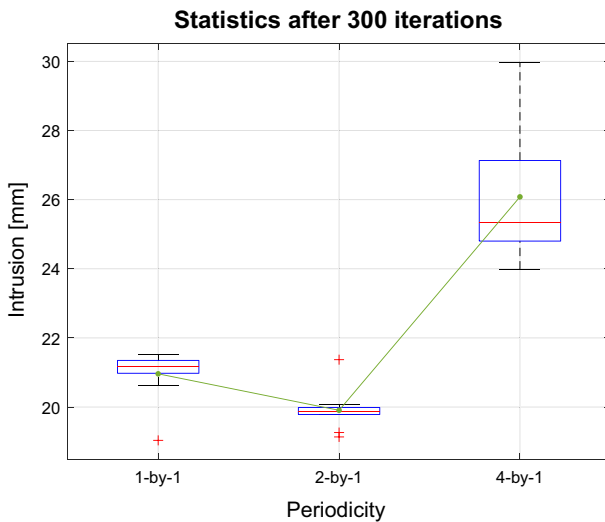
et al. 2018; Raponi et al. 2019) as well as the structures obtained with commercial TO software such as LS-TaSC (Bujny 2020; LSTC 2011). Instead, the 4-by-1 periodicity enforces a too strong constraint that does not allow to reach such a satisfactory material distribution. This is confirmed by both Figs. 25 and 26. The former illustrates the convergence plot for each examined periodicity, averaged across 10 different optimization runs. The latter shows box plots providing statistics upon reaching the total iteration budget. In both figures, the mean intrusion value of the 4-by-1 periodic layout is significantly higher than that of the non-periodic (1-by-1) and 2-by-1 periodic cases.

In particular, from Fig. 26, it is evident that the highest periodicity leads to much more spread solutions at the end of the budget, as indicated by the wider 25th-75th percentile box and whiskers. This might imply that various optimization runs have converged towards diverse local optima, or that the designated total budget might not be large enough to fine-tune the optimal solution for this specific periodicity scenario. Nonetheless, we did identify a shared pattern among the layouts delivering the most favorable intrusion values among the 10 optimization repetitions. In these cases, the optimized RUCs all exhibit layouts reminiscent of a sandwich structure, complemented by a cross-beam reinforcement situated at the center. While the performance of the resulting overall component may not be entirely satisfactory for the considered loading and boundary conditions, it is probable that it possesses greater robustness compared to the optimal arrangements for the 1-by-1 and 2-by-1 periodicity under different and potentially multiple loading conditions.

Figure 27 depicts the distribution of von Mises stress during the loading phase, captured at the time step corresponding to the maximum deformation of the structure. Here we can stress two main aspects. Firstly, in contrast to the static scenarios examined in this study, the performance of the 2-by-1 optimized periodic topology is comparable and even superior to that of the non-periodic layout. Hence, the enforced structural periodicity still allows to maintain flexibility and efficiency within the optimization process. Secondly, the rationale behind the optimal layout achieved in the 4-by-1 periodic scenario becomes evident when analyzing the stress distribution. The most highly stressed sections constitute a substructure that has already been identified as a local optimum in earlier research pertaining to the non-periodic case (Bujny et al. 2018; Raponi et al. 2019). However, the imposed periodicity, coupled with the 50%

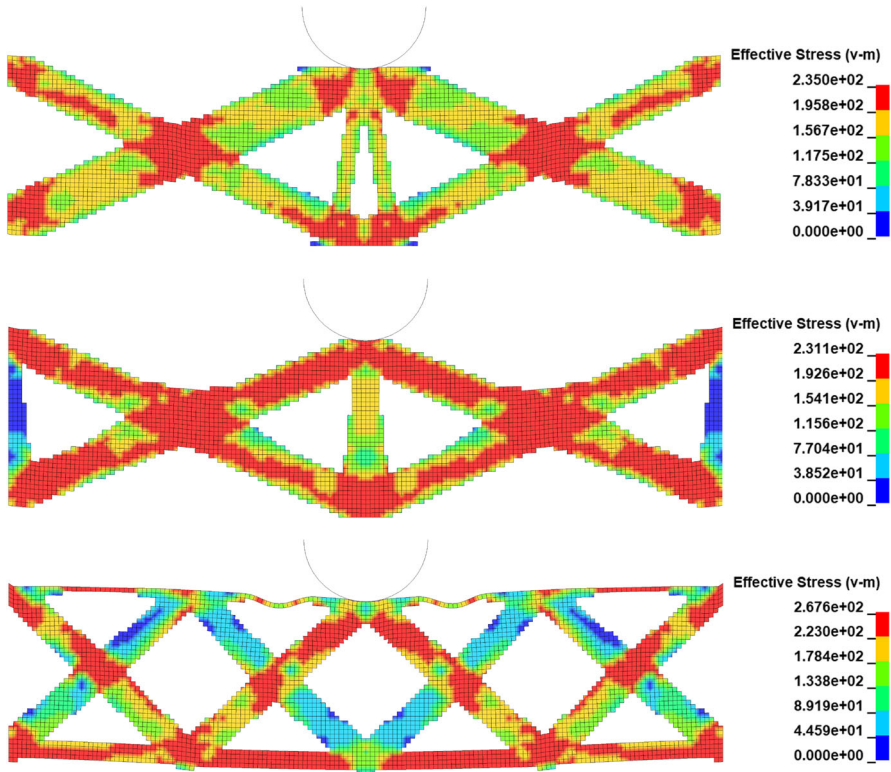


**Fig. 25** Convergence plot illustrating the reduction of intrusion values in a 300-iterations budget, averaged over 10 optimization runs



**Fig. 26** Distribution of 10 final intrusion values in each box plot column for the transverse bending test case with periodicities of 1-by-1, 2-by-1, and 4-by-1

volume constraint, prevents an optimal material distribution. In fact, this leads to the placement of unstressed material that could otherwise reinforce the layout that is actually absorbing the energy generated by the external load.



**Fig. 27** Von Mises stress distribution (in MPa) during the crash event, corresponding to the best design for periodicities of 1-by-1, 2-by-1, and 4-by-1

## 6 Summary

In this paper, we propose a non-gradient macroscopic optimization method for periodic structures, the P-EA-LSM. Thanks to the utilization of evolutionary optimization algorithms, P-EA-LSM is able to address a wide range of structural TO problems involving arbitrary quantifiable objective functions and constraints. This research was motivated by the fact that periodic structures are widely used in structural designs due to their ease of fabrication and energy-absorbing properties. In the context of PTO, only a RUC is optimized and additional periodic constraints are imposed on the optimization formulation to ensure that the optimized structure comprises an array of a prescribed number of identical unit cells. This strategy significantly reduces the number of design variables from thousands to tens, compared to the standard grid representations as for density-based TO methods.

Based on the presented numerical results, we are able to draw the following conclusions: First, P-EA-LSM can yield solutions consistent with other well-established TO techniques (SIMP and BESO) in the existing literature. Second, P-EA-LSM is capable of optimizing layouts of periodic structures with a very low number of design variables. Therefore, using EAs in this context is much more efficient, since it allows for analyzing topologically complex structures based on relatively simple base units. Such designs cannot be easily obtained by traditional density-based optimization methods using the same order of design variables. Third, the mean compliance value rises with the number of unit cells because of the increasing periodicity. The limiting case of  $N_{UC} = 1 \times 1$ , which has no explicit periodic constraint, produces the best final solution with the smallest mean compliance value as expected, but may sacrifice the manufacturability. Indeed, the increase in compliance is the price paid for the extra periodic constraint on the final topology. Finally, application of P-EA-LSM in complex crash TO problems is very promising, which we demonstrated in a 2D scenario of rectangular beam under an impact loading. The method was able to successfully reduce the intrusion of the impactor into the structure for each of the considered periodicities.

For further developments based on this research, one could extend the P-EA-LSM to consider arbitrarily complex cases of TO like those encountered in multiphysics problems, where gradient-based optimizers are not suitable, because of the generic character of the proposed approach. Additionally, to alleviate the problem of high computational costs when using the P-EA-LSM, a surrogate-based approach (Raponi et al. 2019) can be explored. The periodic parameterization with RUCs allows the construction of complex periodic structures while keeping the dimensionality of the optimization problem low. Therefore, surrogate-based optimization techniques appear to be very promising in this context as they suffer from a hampered convergence rate with increasing problem dimensionality, but converge faster at a low dimension, allowing to find competitive designs with a small budget of objective function evaluations, i.e., FEAs. In particular, Bayesian optimization (Moćkus 1975) is very competitive up to 20 variables and often performs better than other heuristics such as ESSs, thanks to its more exploratory behavior in the early phase of the optimization run.

A future challenge is to address 3D TO problems based on P-EA-LSM. In our past works, we demonstrated that the non-periodic variant of P-EA-LSM, i.e., EA-LSM, is suitable for solving both linear elastic and complex, non-linear dynamic crash TO problems in 3D (Bujny 2020; Bujny et al. 2021). Since P-EA-LSM introduces a modification of EA-LSM on the representation level while inheriting the optimization methodology, it should be also capable of addressing 3D problems. By benefiting from the reduced dimensionality of the periodic parametrization, the computational costs of P-EA-LSM are considerably reduced while maintaining structural complexity, and therefore, it could prove itself to be a valuable tool in industrial practice, where periodic structures gain interest, especially for structures under impact loading (Schaedler et al. 2014; Najmon et al. 2018; Liu et al. 2021; Jia et al. 2021).

**Funding** Open Access funding enabled and organized by Projekt DEAL.

**Open Access** This article is licensed under a Creative Commons Attribution 4.0 International License, which permits use, sharing, adaptation, distribution and reproduction in any medium or format, as long as you give appropriate credit to the original author(s) and the source, provide a link to the Creative Commons licence,

and indicate if changes were made. The images or other third party material in this article are included in the article's Creative Commons licence, unless indicated otherwise in a credit line to the material. If material is not included in the article's Creative Commons licence and your intended use is not permitted by statutory regulation or exceeds the permitted use, you will need to obtain permission directly from the copyright holder. To view a copy of this licence, visit <http://creativecommons.org/licenses/by/4.0/>.

## References

- (2014) LS-DYNA R7.1.1. <http://www.lstc.com/products/ls-dyna>
- Bendsøe MP (1989) Optimal shape design as a material distribution problem. *Struct Optim* 1:193–202. <https://doi.org/10.1007/bf01650949>
- Bendsøe MP, Kikuchi N (1988) Generating optimal topologies in structural design using a homogenization method. *Comput Methods Appl Mech Eng* 71:197–224. [https://doi.org/10.1016/0045-7825\(88\)90086-2](https://doi.org/10.1016/0045-7825(88)90086-2)
- Bendsøe MP, Sigmund O (1999) Material interpolation schemes in topology optimization. *Arch Appl Mech (Ing Arch)* 69:635–654. <https://doi.org/10.1007/s004190050248>
- Bendsøe MP, Sigmund O (2004) *Topology optimization: theory, methods, and applications*. Springer, Berlin. <https://doi.org/10.1007/978-3-662-05086-6>
- Bujny M (2020) Level set topology optimization for crashworthiness using evolutionary algorithms and machine learning. Ph.D. Thesis, Technische Universität München. [https://mediatum.ub.tum.de/doc/1540709/vy2vkgzacl23dvm0lr7953oww.PhD\\_thesis\\_Mariusz\\_Bujny.pdf](https://mediatum.ub.tum.de/doc/1540709/vy2vkgzacl23dvm0lr7953oww.PhD_thesis_Mariusz_Bujny.pdf)
- Bujny M, Aulig N, Olhofer M, Duddeck F (2016) Hybrid evolutionary approach for level set topology optimization. In: IEEE congress on evolutionary computation (CEC). IEEE. <https://doi.org/10.1109/cec.2016.7748335>
- Bujny M, Aulig N, Olhofer M, Duddeck F (2018) Identification of optimal topologies for crashworthiness with the evolutionary level set method. *Int J Crashworthiness* 23:395–416. <https://doi.org/10.1080/13588265.2017.1331493>
- Bujny M, Olhofer M, Aulig N, Duddeck F (2021) Topology optimization of 3d-printed joints under crash loads using evolutionary algorithms. *Struct Multidiscip Optim* 64:4181–4206. <https://doi.org/10.1007/s00158-021-03082-z>
- Chen Y, Zhou S, Li Q (2010) Multiobjective topology optimization for finite periodic structures. *Comput Struct* 88:806–811. <https://doi.org/10.1016/j.compstruc.2009.10.003>
- Chen W, Tong L, Liu S (2017) Concurrent topology design of structure and material using a two-scale topology optimization. *Comput Struct* 178:119–128. <https://doi.org/10.1016/j.compstruc.2016.10.013>
- Coello CAC (2002) Theoretical and numerical constraint-handling techniques used with evolutionary algorithms: a survey of the state of the art. *Comput Methods Appl Mech Eng* 191:1245–1287. [https://doi.org/10.1016/s0045-7825\(01\)00323-1](https://doi.org/10.1016/s0045-7825(01)00323-1)
- Deshpande VS, Fleck NA, Ashby MF (2001) Effective properties of the octet-truss lattice material. *J Mech Phys Solids* 49:1747–1769. [https://doi.org/10.1016/s0022-5096\(01\)00010-2](https://doi.org/10.1016/s0022-5096(01)00010-2)
- Duddeck F (2007) Multidisciplinary optimization of car bodies. *Struct Multidiscip Optim* 35:375–389. <https://doi.org/10.1007/s00158-007-0130-6>
- Fu YF, Rolfe B, Chiu LN, Wang Y, Huang X, Ghabraie K (2020) Semdot: smooth-edged material distribution for optimizing topology algorithm. *Adv Eng Softw* 150:102921. <https://doi.org/10.48550/arXiv.2005.09233>
- Fu YF, Rolfe B, Rolfe B (2023) On non-penalization semdot using discrete variable sensitivities. *J Optim Theory Appl* 198:644–677. <https://doi.org/10.1007/s10957-023-02222-3>
- Guo X, Zhang W, Zhong W (2014) Doing topology optimization explicitly and geometrically—a new moving morphable components based framework. *J Appl Mech*. <https://doi.org/10.1115/1.4027609>
- Hassani B, Hinton E (1998) A review of homogenization and topology optimization I—homogenization theory for media with periodic structure. *Comput Struct* 69:707–717. [https://doi.org/10.1016/s0045-7949\(98\)00131-x](https://doi.org/10.1016/s0045-7949(98)00131-x)
- Hu J, Yao S, Huang X (2020) Topology optimization of dynamic acoustic-mechanical structures using the ersatz material model. *Comput Methods Appl Mech Eng* 372:113387. <https://doi.org/10.1016/j.cma.2020.113387>



- Huang X (2020) Smooth topological design of structures using the floating projection. *Eng Struct* 208:110330. <https://doi.org/10.1016/j.engstruct.2020.110330>
- Huang X (2021) On smooth or 0/1 designs of the fixed-mesh element-based topology optimization. *Adv Eng Softw* 151:102942. <https://doi.org/10.1016/j.advengsoft.2020.102942>
- Huang X, Xie YM (2007a) Convergent and mesh-independent solutions for the bi-directional evolutionary structural optimization method. *Finite Elem Anal Des* 43:1039–1049. <https://doi.org/10.1016/j.finell.2007.06.006>
- Huang X, Xie YM (2007b) Optimal design of periodic structures using evolutionary topology optimization. *Struct Multidiscip Optim* 36:597–606. <https://doi.org/10.1007/s00158-007-0196-1>
- Jia J, Da D, Hu J, Yin S (2021) Crashworthiness design of periodic cellular structures using topology optimization. *Compos Struct* 271:114164. <https://doi.org/10.1016/j.compstruct.2021.114164>
- Liu C, Zhu Y, Sun Z, Li D, Du Z, Zhang W, Guo X (2018) An efficient moving morphable component (MMC)-based approach for multi-resolution topology optimization. *Struct Multidiscip Optim* 58:2455–2479. <https://doi.org/10.1007/s00158-018-2114-0>
- Liu H, Chng ZXC, Wang G, Ng BF (2021) Crashworthiness improvements of multi-cell thin-walled tubes through lattice structure enhancements. *Int J Mech Sci* 210:106731. <https://doi.org/10.1016/j.ijmecsci.2021.106731>
- LSTC (2011) LS-TaSC—topology and shape computations for LS-DYNA, v2.0
- Michell AGM (1904) LVIII. the limits of economy of material in frame-structures. *Lond Edinb Dublin Philos Mag J Sci* 8:589–597. <https://doi.org/10.1080/14786440409463229>
- Moćkus J (1975) On Bayesian methods for seeking the extremum. In: Optimization techniques IFIP technical conference Novosibirsk, July 1–7, 1974, Springer, Berlin, pp 400–404. [https://doi.org/10.1007/3-540-07165-2\\_55](https://doi.org/10.1007/3-540-07165-2_55)
- Mozumder C, Renaud JE, Tovar A (2012) Topometry optimisation for crashworthiness design using hybrid cellular automata. *Int J Veh Des* 60:100–120. <https://doi.org/10.1504/IJVD.2012.049160>
- Mukhopadhyay T, Adhikari S (2016) Free-vibration analysis of sandwich panels with randomly irregular honeycomb core. *J Eng Mech* 142:06016008. [https://doi.org/10.1061/\(asce\)em.1943-7889.0001153](https://doi.org/10.1061/(asce)em.1943-7889.0001153)
- Najmon JC, Jacob DJ, Wood ZM, Tovar A (2018) Cellular helmet liner design through bio-inspired structures and topology optimization of compliant mechanism lattices. *SAE Int J Transp Saf* 6:217–236. <https://doi.org/10.4271/2018-01-1057>
- Penninger CL, Watson LT, Tovar A, Renaud JE (2010) Convergence analysis of hybrid cellular automata for topology optimization. *Struct Multidiscip Optim* 40:271–282. <https://doi.org/10.1007/s00158-009-0360-x>
- Querin OM, Steven GP, Xie YM (1998) Evolutionary structural optimisation (ESO) using a bi-directional algorithm. *Eng Comput* 15:1031–1048. <https://doi.org/10.1108/02644409810244129>
- Querin OM, Young V, Steven GP, Xie YM (2000) Computational efficiency and validation of bi-directional evolutionary structural optimisation. *Comput Methods Appl Mech Eng* 189:559–573. [https://doi.org/10.1016/s0045-7825\(99\)00309-6](https://doi.org/10.1016/s0045-7825(99)00309-6)
- Rao SS (2019) *Engineering Optimization: Theory and Practice*. Wiley, New York. <https://doi.org/10.1002/9781119454816>
- Raponi E, Bujny M, Olhofer M, Aulig N, Boria S, Duddeck F (2019) Kriging-assisted topology optimization of crash structures. *Comput Methods Appl Mech Eng* 348:730–752. <https://doi.org/10.1016/j.cma.2019.02.002>
- Schaedler TA, Ro CJ, Sorensen AE, Eckel Z, Yang SS, Carter WB, Jacobsen AJ (2014) Designing metallic microlattices for energy absorber applications. *Adv Eng Mater* 16:276–283. <https://doi.org/10.1002/adem.201300206>
- Schwefel HP (1987) Collective phenomena in evolutionary systems. [https://www.researchgate.net/publication/216301411\\_Collective\\_phenomena\\_in\\_evolutionary\\_systems](https://www.researchgate.net/publication/216301411_Collective_phenomena_in_evolutionary_systems)
- Sigmund O (1994a) Design of material structures using topology optimization. Ph.D. Thesis, Technical University of Denmark. [https://www.researchgate.net/profile/Ole-Sigmund/publication/261173987\\_Design\\_of\\_Material\\_Structures\\_Using\\_Topology\\_Optimization/links/55de078b08aeaa26af0f20d3/Design-of-Material-Structures-Using-Topology-Optimization.pdf](https://www.researchgate.net/profile/Ole-Sigmund/publication/261173987_Design_of_Material_Structures_Using_Topology_Optimization/links/55de078b08aeaa26af0f20d3/Design-of-Material-Structures-Using-Topology-Optimization.pdf)
- Sigmund O (1994b) Materials with prescribed constitutive parameters: an inverse homogenization problem. *Int J Solids Struct* 31:2313–2329. [https://doi.org/10.1016/0020-7683\(94\)90154-6](https://doi.org/10.1016/0020-7683(94)90154-6)
- Sigmund O (1995) Tailoring materials with prescribed elastic properties. *Mech Mater* 20:351–368. [https://doi.org/10.1016/0167-6636\(94\)00069-7](https://doi.org/10.1016/0167-6636(94)00069-7)

- Sigmund O (2000) Topology optimization: a tool for the tailoring of structures and materials. *Philos Trans R Soc Lond Ser A* 358:211–227. <https://doi.org/10.1098/rsta.2000.0528>
- Sigmund O (2001) A 99 line topology optimization code written in MATLAB. *Struct Multidiscip Optim* 21:120–127. <https://doi.org/10.1007/s001580050176>
- Sigmund O, Maute K (2013) Topology optimization approaches. *Struct Multidiscip Optim* 48:1031–1055. <https://doi.org/10.1007/s00158-013-0978-6>
- Sigmund O, Petersson J (1998) Numerical instabilities in topology optimization: a survey on procedures dealing with checkerboards, mesh-dependencies and local minima. *Struct Optim* 16:68–75. <https://doi.org/10.1007/bf01214002>
- Tang Y, Kurtz A, Zhao YF (2015) Bidirectional evolutionary structural optimization (BESO) based design method for lattice structure to be fabricated by additive manufacturing. *Comput Aided Des* 69:91–101. <https://doi.org/10.1016/j.cad.2015.06.001>
- Thomas S (2021) Finite periodic topology optimization with oriented unit-cells data set. <https://doi.org/10.17632/wj6s2d8xbg.2>
- Thomas S, Li Q, Steven G (2020) Topology optimization for periodic multi-component structures with stiffness and frequency criteria. *Struct Multidiscip Optim* 61:2271–2289. <https://doi.org/10.1007/s00158-019-02481-7>
- Thomas S, Li Q, Steven G (2021) Finite periodic topology optimization with oriented unit-cells. *Struct Multidiscip Optim* 64:1765–1779. <https://doi.org/10.1007/s00158-021-03045-4>
- van Dijk NP, Maute K, Langelaar M, van Keulen F (2013) Level-set methods for structural topology optimization: a review. *Struct Multidiscip Optim* 48:437–472. <https://doi.org/10.1007/s00158-013-0912-y>
- Xia L, Xia Q, Huang X, Xie YM (2016) Bi-directional evolutionary structural optimization on advanced structures and materials: a comprehensive review. *Arch Comput Methods Eng* 25:437–478. <https://doi.org/10.1007/s11831-016-9203-2>
- Xie YM, Steven GP (1993) A simple evolutionary procedure for structural optimization. *Comput Struct* 49:885–896. [https://doi.org/10.1016/0045-7949\(93\)90035-C](https://doi.org/10.1016/0045-7949(93)90035-C)
- Xie YM, Zuo ZH, Huang X, Rong JH (2011) Convergence of topological patterns of optimal periodic structures under multiple scales. *Struct Multidiscip Optim* 46:41–50. <https://doi.org/10.1007/s00158-011-0750-8>
- Yang XY, Xie YM, Steven GP, Querin OM (1999) Bi-directional evolutionary method for stiffness optimization. *AIAA J* 37:1483–1488. <https://doi.org/10.2514/2.626>
- Zhang W, Sun S (2006) Scale-related topology optimization of cellular materials and structures. *Int J Numer Methods Eng* 68:993–1011. <https://doi.org/10.1002/nme.1743>
- Zhang W, Yuan J, Zhang J, Guo X (2015) A new topology optimization approach based on moving morphable components (MMC) and the ersatz material model. *Struct Multidiscip Optim* 53:1243–1260. <https://doi.org/10.1007/s00158-015-1372-3>
- Zhang W, Zhou J, Zhu Y, Guo X (2017) Structural complexity control in topology optimization via moving morphable component (MMC) approach. *Struct Multidiscip Optim* 56:535–552. <https://doi.org/10.1007/s00158-017-1736-y>
- Zheng Y, Xiao M, Gao L, Li H (2018) Robust topology optimization for periodic structures by combining sensitivity averaging with a semianalytical method. *Int J Numer Methods Eng* 117:475–497. <https://doi.org/10.1002/nme.5964>
- Zuo ZH (2009) Topology optimization of periodic structures. Ph.D. Thesis, Royal Melbourne Institute of Technology. <https://core.ac.uk/download/pdf/15614989.pdf>

**Publisher's Note** Springer Nature remains neutral with regard to jurisdictional claims in published maps and institutional affiliations.